Electronic Supplementary Material (ESI) for Chemical Communications.
This journal is © The Royal Society of Chemistry 2022

Supplementary Information for

Synergistically Promoted Charge Separation/Transfer in ZnO Nanosheet Photoanode *via* the Incorporation of Multifunctional 3DrGO

Bing He, [‡a] Hexuan Sheng, [‡a] Qian Liu,[a] Zhifu Hu,[a] Jingnan Wang,[a] Xiaoqin Hu,*[a] Yingkui Yang,[b] Yang Wang, *[a] Zhen Li,[a] and Xueqin Liu*[a]

[a] Faculty of Materials Science and Chemistry, China University of Geosciences, Wuhan 430074, PR China

[b] Key Laboratory of Catalysis and Energy Materials Chemistry of Ministry of Education & Hubei Key Laboratory of Catalysis and Materials Science, South-Central University for Nationalities, Wuhan 430074, China

* E-mails: liuxq@cug.edu.cn (X.Q. Liu)

[1] These authors contributed equally to this work.

Experimental

Preparation of ZnO photoanode.

The ZnO photoanode was fabricated by an electrochemical deposition method. [1] The electrochemical deposition progress was performed by an electrochemical workstation (CHI 650E, Shanghai) and a three-electrode cell. The cleaned FTO (F-doped SnO_2 coated glass), standard calomel electrode (SCE), and Pt foil were served as the working electrode, reference electrode, and counter electrode, respectively. The electrolyte was prepared by dissolving 0.15 M $Zn(NO_3)_2$ and 0.1 M KCl. The cathodic deposition was performed potentiostatically at -1.0 V vs. SCE at 75 ℃ with varying deposition times (6-12 min).

Preparation of 3DrGO electrode.

The electrochemical reduction process was used to fabricate the 3DrGO electrode.[2] The FTO was immersed in 0.5% (v/v) 3-Amino-propyltriethoxysilane ethanol solution for 1 h at room temperature and dried in an oven at 120 ℃ before used to increase adhesion. The immersed FTO, a standard calomel electrode (SCE), and a Pt foil were served as the working electrode, reference electrode, and the counter electrode, respectively. Electrodeposition of 3DrGO on the FTO electrodes was carried out in a suspension of 4 mg/mL graphene oxide solution containing 0.12 M $LiClO_4$ at an external potential of -1.0 V vs. SCE for 150 s. Further to reduce 3DrGO nanosheets, the as-prepared electrode was electrochemically reduced in a 0.1 M KCl solution for 10 cycles using a cyclic voltammetry scan with a potential range of 0 to 1.5 V vs. SCE at a rate of 50 mV s^{-1}. Then the 3DrGO electrode was cleaned with deionized water and preserved by soaking in deionized water.

Preparation of ZnO/3DrGO photoanode.

The preparation method of ZnO/3DrGO photoanode is similar to that of ZnO photoanode. The ZnO nanosheets were electrodeposited on the surface of the as-prepared 3DrGO electrode.

Preparation of ZnO/rGO photoanode.

To obtain rGO, the 3DrGO electrode was dried in a vacuum oven at 60 °C for 12 hours.

The ZnO nanosheets were electrodeposited on the surface of rGO to obtain the ZnO/rGO photoanode.

Characterization

A field-emission scanning electron microscope (FESEM, SU8010) connected with an X-ray energy-dispersive spectrometer (EDS) and transmission electron microscope (TEM, Talos F200S) were used to examine the surface morphology of as-prepared photoanodes. Images were taken using a transmission electron microscope (TEM, Talos F200S) with a 120 kV acceleration voltage. A Bruker D8 Advanced X-ray diffractometer was used to analyze the structural properties of the materials (XRD, Bruker AXS D8-Focus). The surface bonding information of photoanode materials was analyzed using X-ray photoelectron spectroscopy (XPS, Physical Electronics PHI 1600 ESCA). Raman spectra of as-perpared samples were measured by an automatic microscopic Raman spectrometer (HORIBA XploRA plus). The light absorption properties of as-prepared samples were measured by a UV-Vis diffuse reflectance spectrometer (UV-2550PC spectrophotometer). The photoluminescence (PL) studies were carried out by a Fluoromax 4P spectrofluorometer (Horiba) with a light (λ = 350 nm). The value of temperature and infrared image were recorded by an infrared thermography.

PEC measurements

The general PEC test system for water splitting was calculated according to our previous works.[3] The electrolyte uses the 0.5 M phosphate buffer solution (KPi, pH 7). All photoanodes were illuminated by simulated sunlight from the FTO side, while the 808 nm NIR laser comes from the front side of photoanodes. The photocurrent-potential curves were measured by scanning with a continuous voltage change at a scan rate of 10 mV s^{-1}.

The incident photon-to-current conversion efficiency (IPCE) was measured at 1.23 V_{RHE} with a 300 W Xe arc lamp and a monochromator in KPi solution (pH 7). During reaction, the output of H_2 or O_2 was collected every 30 min at 1.23 V_{RHE} using a

GC7920 gas chromatography in an airtight N_2 flow system. The Mott-Schottky (MS) plots were made in the dark with an amplitude of 10 mV and a frequency of 1000 Hz. Applying a modest AC amplitude of 50 mV throughout a frequency range of 10^4 to 10^{-2} Hz at 1.23 V_{RHE} was used to perform electrochemical impedance spectroscopy (EIS) measurements. The intensity-modulated photocurrent spectroscopy (IMPS) measurement was conducted by using an electrochemistry workstation (Zahner PP211) and an LED source (365 nm) under a light intensity of 80 mW cm^{-2}. The frequency range is from 10 KHz to 10 mHz and the amplitude of ac perturbation signal was set to a 10% of the constant light intensity.

The Faradaic efficiency was calculated by dividing the amount of gas detected by the theoretical amount of gas calculated on the basis of the total charge passed, using the equations (1):

$$FE(\%) = \frac{A \times n(mol) \times F(C\ mol^{-1})}{I \times t} \times 100\% \quad (1)$$

where n is moles of evolved H_2 or O_2 gas, A is the number of electrons required to generate one H_2 or O_2 molecule (two for H_2, four for O_2) and F is the Faraday constant (96485.33 C mol^{-1}).

Charge separation efficiency (η)

The η_{sep} (related to the bulk charge separation efficiency) could be determined using the equations (2):

$$\eta_{sep} = \frac{J_{sulfite}}{J_{abs}} \times 100\% \quad (2)$$

where $J_{sulfite}$ is the photocurrent density in the electrolyte with sulfite oxidation. The J_{abs} of ZnO/FTO and ZnO/3D rGO/FTO with or without NIR light are 0.52, 1.43 and 2.03 mA cm^{-2}, which were calculated by the overlapped area integration of standard solar absorption spectrum and UV-Vis absorption spectrum, respectively (Fig. S5).

Carrier concentration (N_d)

The N_d of ZnO/FTO and ZnO/3DrGO/FTO photoanodes with or without NIR light irradiation was obtained from the Mott-Schottky (MS) plots by equation (3):

$$N_d = \frac{2}{e\varepsilon\varepsilon_0}\left[\frac{d(1/C^2)}{d\upsilon}\right]^{-1} \quad (3)$$

where e is the electron charge (1.60×10^{-19} C), ε is the dielectric constant of ZnO (7.8), ε_0 is the permittivity of free space (8.85×10^{-12} F m^{-1}) and $d(1/C^2)/d\upsilon$ is the slope of the curve shown in MS plots (Fig. 3b).

Carrier transfer time (τ_d)

The carrier transfer time (τ_d) of photoanodes was obtained from IMPS by the equation (4):

$$\tau_d = \frac{1}{2\pi f_{min}} \quad (4)$$

where f_{min} is the corresponding frequency of the lower semicircular arc's lowest point in IMPS curves.

Rate constants (k)

The rate constants (k) were extracted by using equations (5-6) from the IMPS data at different applied potentials,

$$K_{tr}/(K_{tr} + K_r) = X \quad (5)$$

$$K_{tr} + K_r = 2\pi f_{max} \quad (6)$$

where K_{tr} is the charge transport rate constant, K_r is charge recombination rate constant, X is the X-intercept at the low frequency range of the upper semicircular arc, f_{max} is the corresponding frequency of the highest point in the upper semicircular arc.

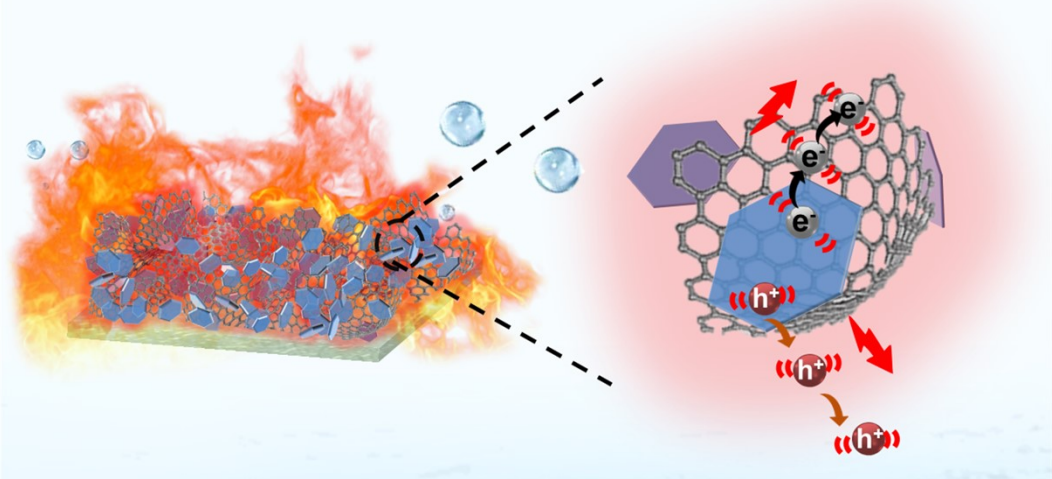

Scheme 1 Schematic illustration of photothermal enhanced ZnO/3DrGO photoanode for PEC water splitting.

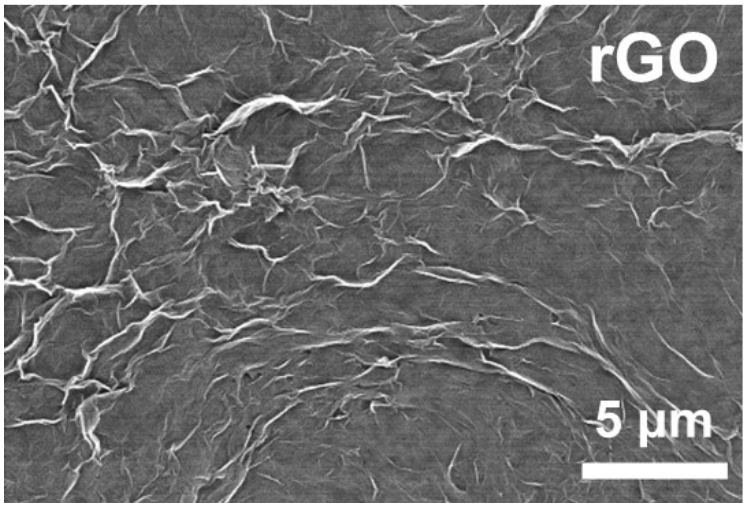

Fig. S1 SEM images of rGO/FTO.

Compared with rGO, the three-dimensional porous structure of the 3DrGO nanosheet significantly increases the area for receiving incident light and improves the utilization efficiency of NIR light in irradiation. On the other hand, the contact area of 3DrGO with ZnO nanosheets is more than that of the planar structure, which enables uniform heating.

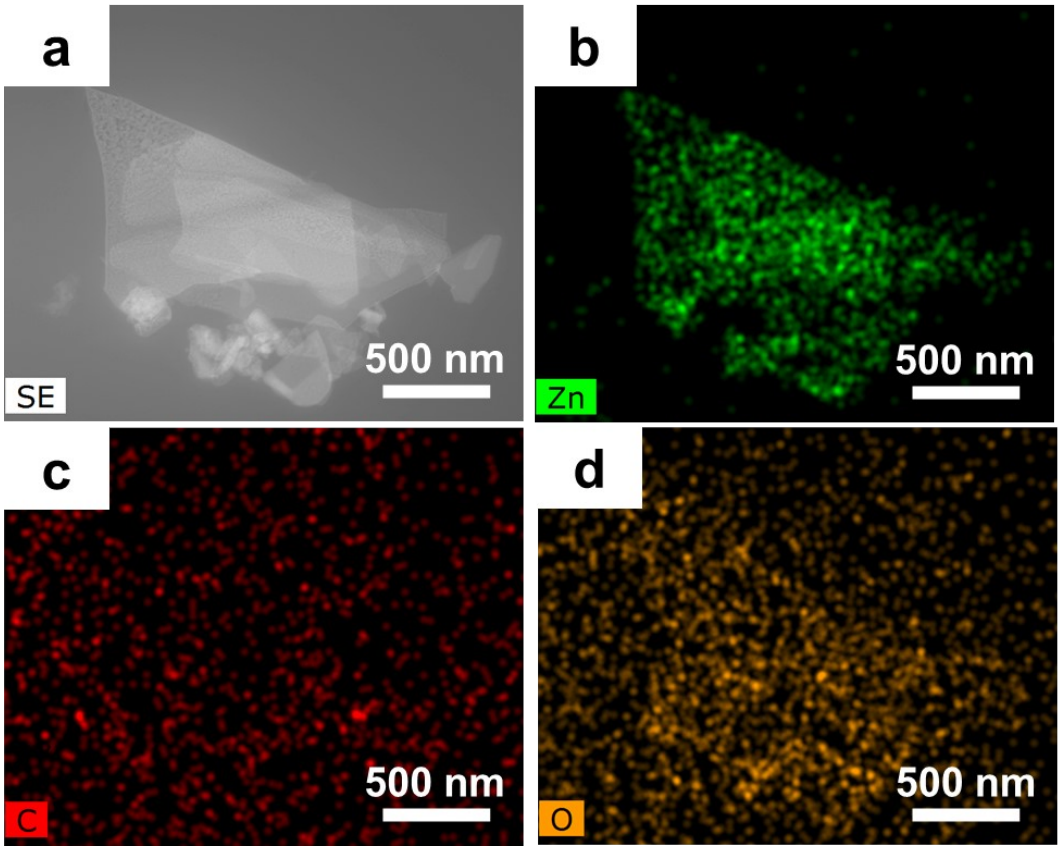

Fig. S2 Elemental mapping of Zn, C and O for ZnO/3DrGO photoanode.

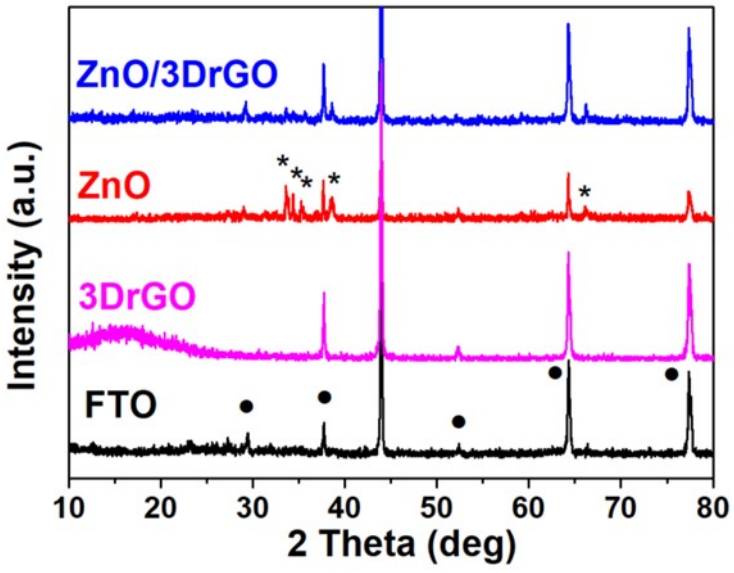

Fig. S3 XRD patterns of FTO, 3DrGO, ZnO and ZnO/3DrGO photoelectrodes.

The diffraction peaks at 30.79°, 34.29°, 35.35° and 66.26°, corresponding to (100), (002), (101), and (112) planes of ZnO, are indexed to the hexagonal zincite structure (JCPDS No. 75-1533). These characteristic peaks can be also observed in ZnO/3DrGO

photoanode, clearly demonstrating the deposition of ZnO on 3DrGO.

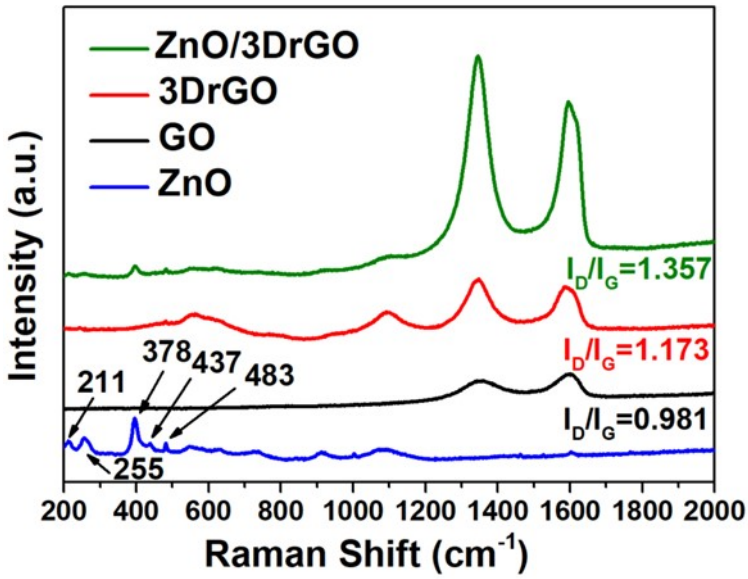

Fig. S4 Raman spectra of ZnO, GO, 3DrGO and ZnO/3DrGO photoelectrodes.

The peaks at 211, 255, 378, 437, and 483 cm^{-1} are assigned to the ZnO nanosheets, which could be also found in the spectrum of ZnO/3DrGO. In addition, the Raman spectra of GO, 3DrGO, and ZnO/3DrGO display strong D band and G band of graphene at ~1342 and ~1600 cm^{-1}, indicating a successful hybridization of ZnO and 3DrGO.

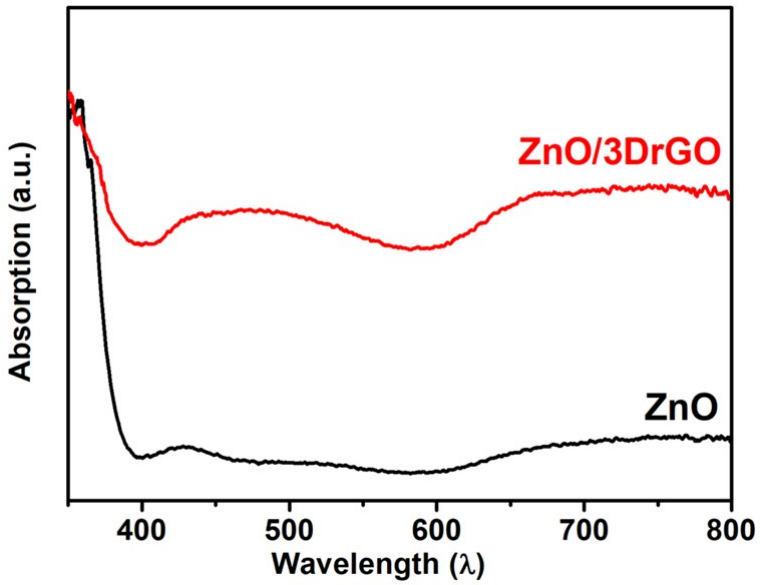

Fig. S5 UV-vis absorption spectra of ZnO and ZnO/3DrGO photoamodes.

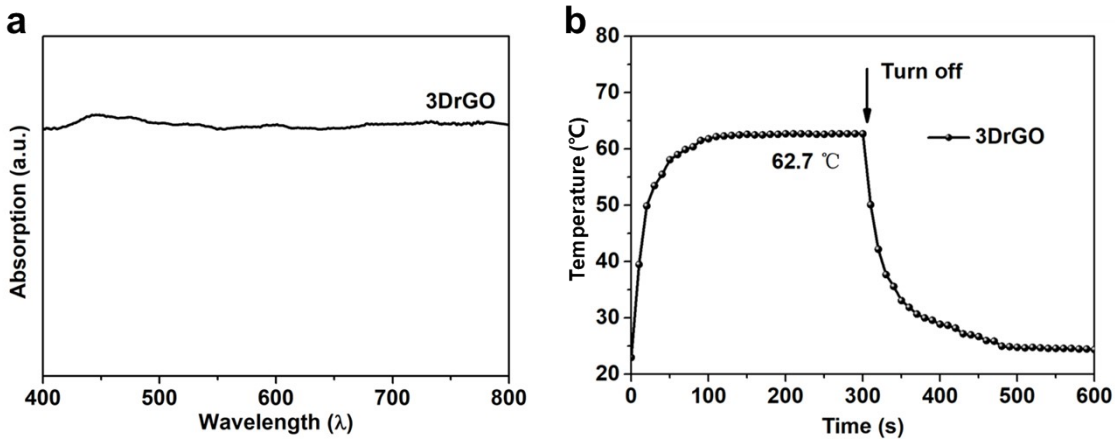

Fig. S6 (a) UV-vis absorption spectra of 3DGO electrode. (b) Temperature evaluation of 3DrGO electrode with 808 nm laser irradiation at 5 W cm^{-2} for different times.

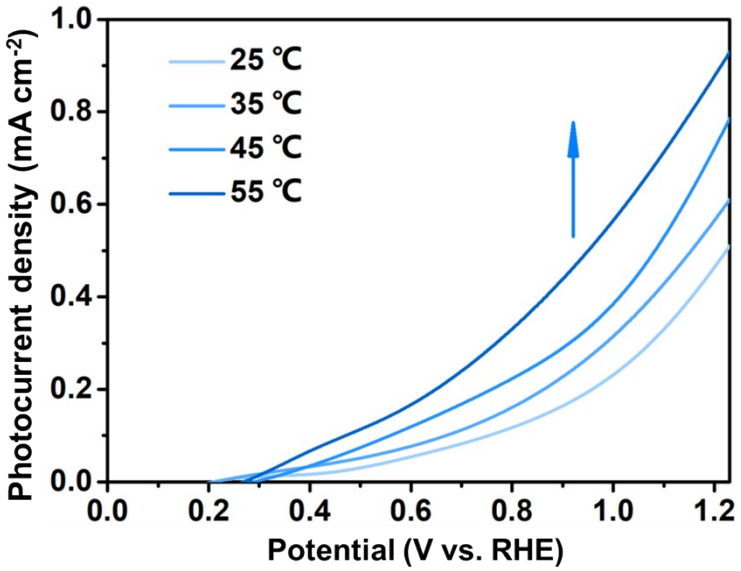

Fig. S7 LSV curves of ZnO photoanode was evaluated at different electrolyte temperatures

The temperature value of the electrolyte was recorded by thermocouple. When the temperature rises from 25 °C to 45 °C, the photocurrent density of the ZnO photoanode increases significantly, indicating the increase of operating temperature is an effective way to improve the PEC performance of ZnO photoanode.

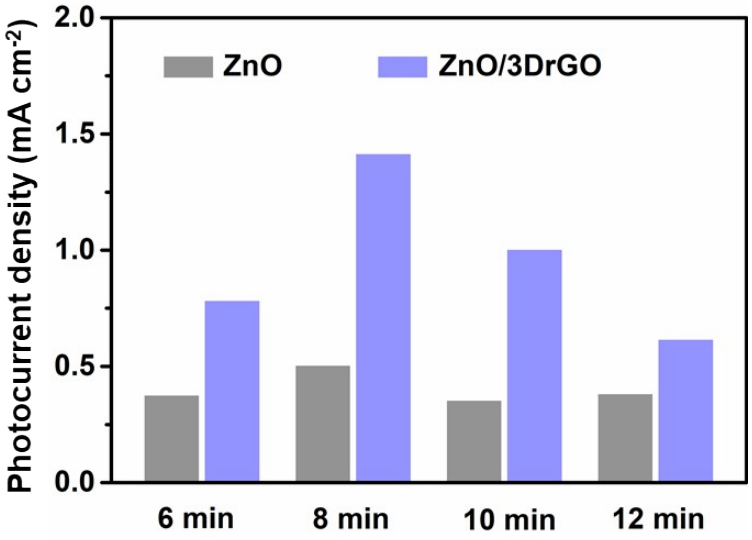

Fig. S8 Photoanode current of ZnO and ZnO/3DrGO photoanodes with different deposition times of ZnO (6 min, 8 min, 10 min, and 12 min) at 1.23 V_{RHE}.

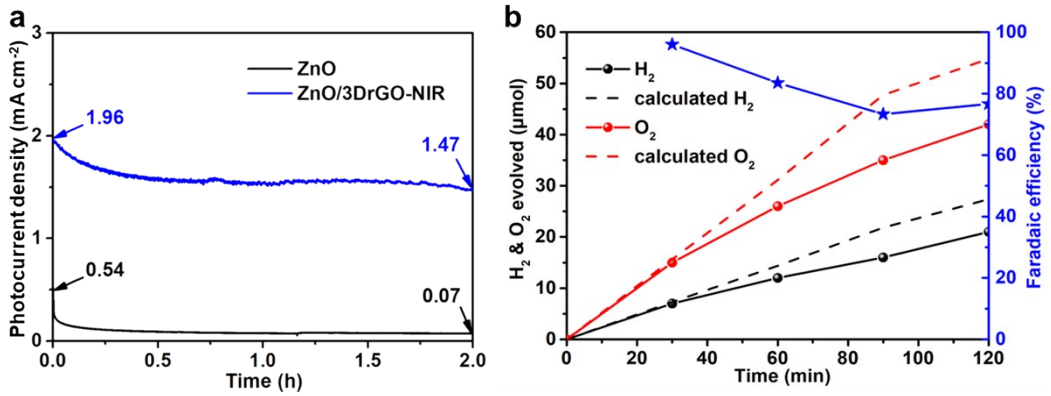

Fig. S9 (a) I-t curves of ZnO and ZnO/3DrGO-NIR photoanodes. (b) The H_2 and O_2 evolution of ZnO/3DrGO-NIR at 1.23 V_{RHE} under AM 1.5G illumination.

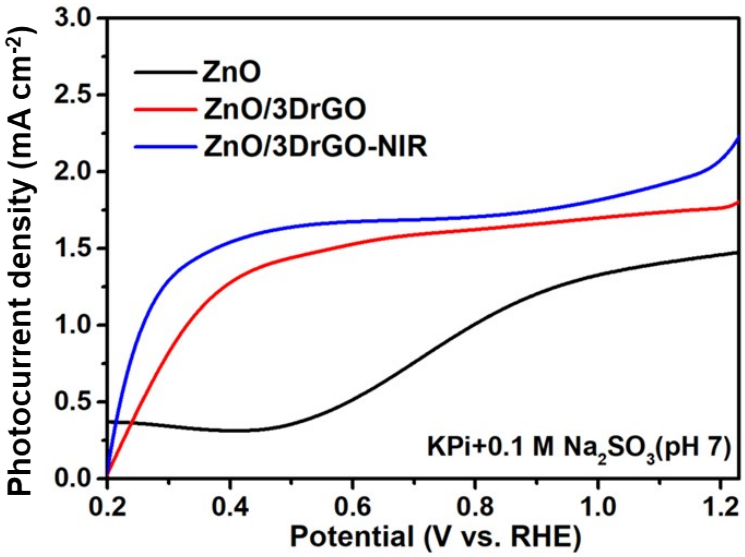

Fig. S10 LSV curves of ZnO and ZnO/3DrGO photoanodes measured with Na_2SO_3 in the electrolyte.

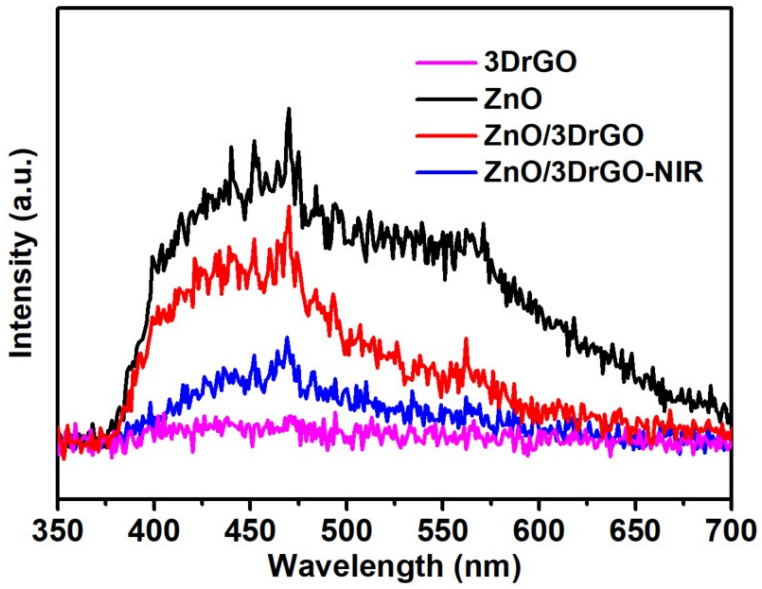

Fig. S11 Photoluminescence (PL) spectra of 3DrGO electrode, ZnO, ZnO/3DrGO, ZnO/3DrGO-NIR photoanodes.

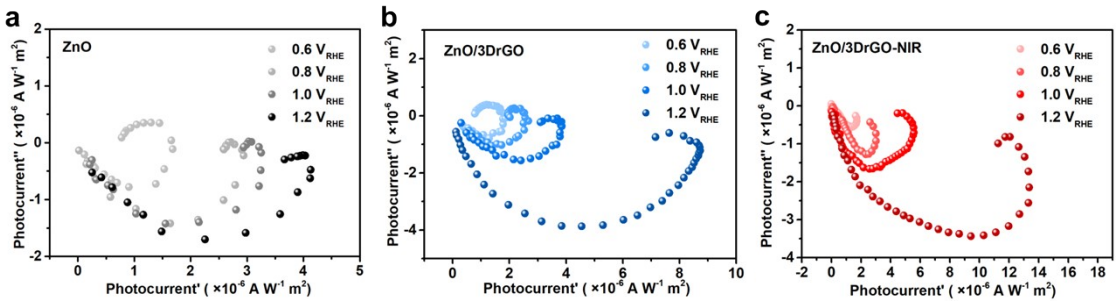

Fig. S12 IMPS Nyquist plots at different applied potentials of (a) ZnO, (b) ZnO/3DrGO and (c) ZnO/3DrGO-NIR photoanodes.

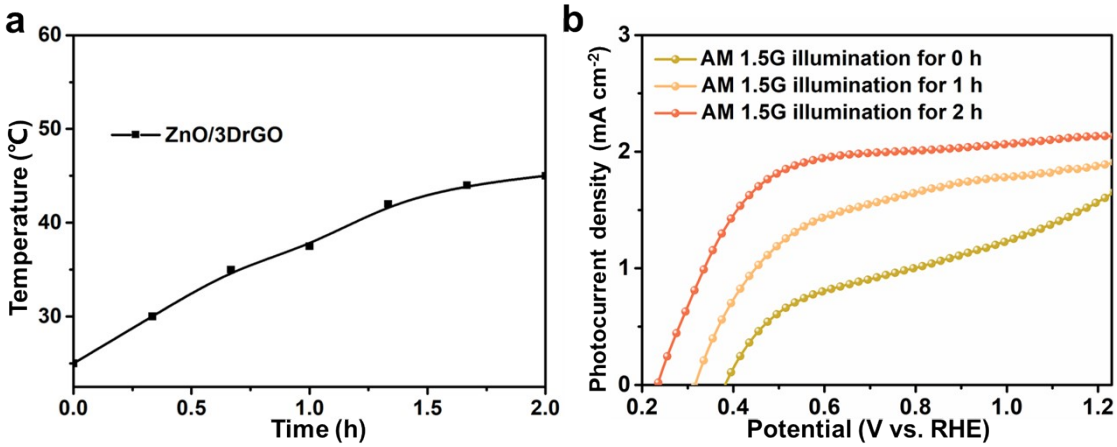

Fig. S13 (a) Temperature-time curves and (b) LSV curves under light illumination (AM 1.5G) of ZnO/3DrGO photoanode for different irradiation of time.

The photogenerated electrons are transferred rapidly from ZnO to the surface of 3DrGO and eventually to FTO glass because of the high conductivity and 3D porous structure of 3DrGO. Correspondingly, the carrier concentration also increases significantly. After irradiation with a NIR laser, the operation temperature of the ZnO/3DrGO photoanode is elevated moderately in situ. The photothermal effect of the 3DrGO nanosheets leads to effective charge transport for both electrons and holes and a dramatically decreased charge recombination rate after NIR laser irradiation, as validated by MS, EIS, and IMPS data. Therefore, the high conductivity, 3D porous structure and photothermal effect of 3DrGO have a synergistic effect on the PEC performance of the ZnO/3DrGO photoanode, resulting in enhanced water splitting efficiency.

Table S1 Comparison of the photocurrent density (J (mA cm^{-2})) with the reported most active ZnO-based photoanodes obtained at 1.23 V_{RHE}.

Photoanode	Electrolyte	J (mA cm^{-2})	Year	Ref.
FTO/ZnO/rGO/M-Bi	K-Bi buffer solution (pH 9.2)	~0.86	2018	4
FTO/Y:ZnO/PCN	0.5 M Na_2SO_4	~0.40	2018	5
FTO/ZnO/$FeVO_4$	0.5 M Na_2SO_4 (pH 6.5)	~2.05	2019	6
FTO/ZnO/GaON	0.5 M KOH	~2.25	2019	7
FTO/ZnO/NCD@ZIF-8	0.5 M Na_2SO_4 (pH 6.8)	~0.45	2019	8
FTO/ZnO/$ZnWO_4$/NiOOH	0.02 M KOH (pH 12.3)	~1.70	2019	9
FTO/ZnO/CdS	0.5 M Na_2SO_4 (pH 7.35)	~1.50	2019	10
FTO/ZnO/Au	0.5 M Na_2SO_4 (pH 7)	~1.80	2020	11
FTO/ZnO/V_2O_5	0.5 M Na_2SO_4 (pH 7)	~1.21	2020	12
FTO/ZnO/MoS_x	0.5 M Na_2SO_4 (pH 7)	~2.50	2020	13
FTO/ZnO/CdS/$MoSe_2$	0.55 M Na_2S+0.127 M Na_2SO_3	~2.40	2021	14
Ti/ZnO/GO	0.5 M Na_2SO_3	~4.73	2021	15
FTO/ZnO/$ZnCo_2O_4$	0.5 M Na_2SO_4 (pH 6.4)	~1.58	2021	16
FTO/ZnO/CdO/rGO	0.5 M Na_2SO_4 (pH 7)	~1.15	2021	17
ITO/ZnO/CuI	0.1 M NaOH	~0.67	2022	18
FTO/ZnO-B/CdS	0.5 M Na_2SO_3 at (pH 9)	~1.52	2022	19
ITO/ZnO/In_2S_3	0.5 M Na_2SO_4 (pH 6.89)	~2.40	2022	20
FTO/ZnO/3DrGO-NIR	0.5 M KPi (pH 10)	~2.03		this work

Table S2 The fitting results of R_Ω, R_{ct}, CPE1-T and CPE1-P for different photoanodes in KPi solution by ZVIEW.

Samples	R_Ω(Ω)	R_{ct}(Ω)	CPE1–T	CPE1–P
ZnO	28.9	7539.0	2.9×10^{-5}	0.73
ZnO/3DrGO	26.4	486.5	9.4×10^{-5}	0.80
ZnO/3DrGO-NIR	25.7	282.3	7.6×10^{-5}	0.77

Reference

1. X. Bai, L. Yi, D. Liu, E. Nie, C. Sun, H. Feng, j. Xu, Y. Jin, Z. Jiao and X. Sun, *Appl.Surf. Sci.*, 2011, **257**, 10317-10321.
2. S. Yang, Y. Huang, W. Zhu, B. Deng, H. Wang, Z. Zhang, P. Bao and G. Wang, *Int. J. Hydrogen Energy*, 2014, **39**, 15063-15071.
3. B. He, S. Jia, M. Zhao, Y. Wang, T. Chen, S. Zhao, Z. Li, Z. Lin, Y. Zhao and X. Liu, *Adv. Mater.*, 2021, **33**, e2004406.
4. H. Zhang, W. Tian, Y. Li, H. Sun, M. O. Tadé and S. Wang, *J. Mater. Chem. A*, 2018, **6**, 24149-24156.
5. Y. Fang, Y. Xu, X. Li, Y. Ma and X. Wang, *Angew Chem. Int. Ed. Engl.*, 2018, **57**, 9749-9753.
6. X. Long, L. Gao, F. Li, Y. Hu, S. Wei, C. Wang, T. Wang, J. Jin and J. Ma, *Appl. Catal. B: Environ.*, 2019, **257**, 117813.

7. H.-P. Ma, J.-H. Yang, J.-J. Tao, K.-P. Yuan, P.-H. Cheng, W. Huang, J.-C. Wang, Q.-X. Guo, H.-L. Lu and D. W. Zhang, *Nano Energy*, 2019, **66**, 104089.
8. H. Han, F. Karlicky, S. Pitchaimuthu, S. H. R. Shin and A. Chen, *Small*, 2019, **15**, e1902771.
9. S. Fu, H. Hu, C. Feng, Y. Zhang and Y. Bi, *J. Mater. Chem. A*, 2019, **7**, 2513-2517.
10. H. Guo, C. Su, D. Yu, L. Li, Z. Liu, Z. Han and X. Lu, *J. Electroanalytical Chem.*, 2019, **854**, 113546.
11. C. Mahala, M. D. Sharma and M. Basu, *ACS Appl. Nano Mater.*, 2020, **3**, 1153-1165.
12. T.-F. Hou, M. A. Johar, R. Boppella, M. A. Hassan, S. J. Patil, S.-W. Ryu and D.-W. Lee, *J. Energy Chem.*, 2020, **49**, 262-274.
13. M. D. Sharma, C. Mahala and M. Basu, *Int. J. Hydrogen Energy*, 2020, **45**, 12272-12282.
14. L. Li, H. Shi, H. Yu, X. Tan, Y. Wang, S. Ge, A. Wang, K. Cui, L. Zhang and J. Yu, *Appl. Catal. B: Environ.*, 2021, **292**,120184.
15. A. G. Abd-Elrahim and D.-M. Chun, *J. Alloy. Compd.*, 2021, **870**,159403.
16. D. Maity, K. Karmakar, D. Pal, S. Saha, G. G. Khan and K. Mandal, *ACS Appl. Energy Mater.*, 2021, **4**, 11599-11608.
17. L. Sun, J. Sun, X. Sun, S. Bai, Y. Zhao, R. Luo, D. Li and A. Chen, *J. Colloid Interf. Sci.*, 2021, **608**, 2377-2386.
18. S. Banerjee and R. Thangavel, *Mat. Sci. Semicon. Proc.*, 2022, **146**, 106690.
19. M. Kolaei, M. Tayebi, Z. Masoumi and B.-K. Lee, *J. Alloy. Compd.*, 2022, **906,** 164314.
20. N. Kaur, A. Ghosh, M. Ahmad, D. Sharma, R. Singh and B. R. Mehta, *J. Alloy. Compd.*, 2022, **903**, 164007.